

000
001
002
003
004
005
006
007
008
009
010
011
012
013
014
015054
055
056
057
058
059
060
061
062
063
064
065
066
067
068
069
070
071
072
073
074
075
076
077
078
079
080
081
082
083
084
085
086
087
088
089
090
091
092
093
094
095
096
097
098
099
100
101
102
103
104
105
106
107

Multilayer Coupled Orthogonal Dictionary Learning for Robust Real Image Denoising

Anonymous CVPR submission

Paper ID ****

Abstract

Existing image denoising methods largely depends on noise modeling and estimation. The commonly used noise models, additive white Gaussian or Mixture of Gaussians, are inflexible in describing the complex noise on real noisy images or time consuming in parametric estimation, respectively. Therefore, how to perform image denoising without noise modeling and estimation is an essential while challenging problem. In this paper, we attempt to solve this problem by directly learning the transformation process between the noisy images and clean ones. The transformation is learned on patches instead of images for dimensional tractability. The learning data is collected by constructing paired noisy and clean patches from unpaired real noisy and clean images. Since real noise is signal dependent and from several main sources [1], we cluster the learning data into multiple components. For each component, we learn in an integrated way two paired dictionaries for the noisy and clean data and two transformation functions between them. The overall learned transformation process could remove the noise from different sources. Experiments show that the proposed Paired Dictionary and Transformation Learing (PDTL) model achieves better performance on denoising real noisy images than other noise estimation based methods.

1. Introduction

Image denoising is a fundamental problem in computer vision and image processing. It is an ideal platform for testing natural image models and provides high-quality images for other computer vision tasks such as image registration, segmentation, and pattern recognition, etc. For several decades, there emerge numerous image denoising methods [2, 3, 4, 5, 6, 7, 8, 9, 10, 11, 12, 13, 14, 15, 16, 17, 18, 19], and most of them focus on dealing with additive white Gaussian noise (AWGN). Among these methods, [13, 14, 15, 16, 17, 18, 19] are designed to deal with real

noisy images. Almost all these methods coincidentally employ a two-stage framework: in the first stage, assuming a distribution model (usually Gaussian) on the noise and estimate its parameters; in the second stage, performing denoising with the help of the noise modeling and estimation in the first stage. However, the Gaussian assumption is inflexible in describing the complex noise on real noisy images [15, 19]. Although the mixture of Gaussians (MoG) model is possible to approximate any unknown noise [18], estimating its parameters is often time consuming via nonparametric Bayesian techniques [18] [20]. To avoid the above mentioned problems, it is naturally to ask, whether it is possible to perform denoising on real noisy images without noise modeling and estimation?

To answer this question, we look close into several discriminative learning methods [8, 10, 12] achieving expressive performance on Gaussian noise removal. These methods require a set of paired images, namely clean ground-truth images and the simulated noisy counterparts degraded by identical noise (mainly additive white Gaussian noise, AWGN), to learn an effective model for image denoising. However, the noise in real images are much more complex than Gaussian, since it depends on camera series, brands, as well as the settings (ISO, shutter speed, and aperture, etc). Thus, the model learned with AWGN would become much less effective for denoising real noisy images. What's more, usually real noisy images do not have clean counterparts. Therefore, almost all current discriminative learning methods cannot be directly applied to real noisy images.

The above mentioned limitations indicate that, novel denoising methods are been waiting for which can: 1) avoid noise modeling and estimation; 2) learn without paired training images; 3) deal with complex noise on real noisy images. In this paper, we attempt to solve the three problems in an integrated way for robust real image denoising. Specifically, we collect a comprehensive set of real noisy images and an independent set of clean images, and propose a learning based model to directly transform the noisy input into clean counterparts. The rationale is that, the noise on real noisy images obtained through in-camera imaging

108 pipeline [21] are structure dependent [19] and identified by
109 several main types [1, 22]. To better deal with different structures
110 and noise sources, we propose to learn our model on
111 multile clusters of image patches instead of on a set of large
112 images. Besides, it is difficult to learn models on whole images
113 since that natural images are of high dimensionality.
114 What’s more, for our learning model, though images are
115 different, it is possible to find a cluster of patches in clean
116 images which are similar to given noisy patches. For each
117 cluster of patches, we learn two dictionaries and transformation
118 functions to characterize the structures of and relationship
119 between niosy and clean image patches. We perform
120 comprehensive experiments on real noisy images captured
121 by different CMOS or CCS sensors. The results demon-
122 strate that our method achieves comparable or even better
123 performance on denoising real noisy images. This reveals
124 the potential advantages of dscriminative learning methods
125 on robust and complex real noisy image denoising problem.
126

127 1.1. Our Contributions

128 The contributions of this paper are closely related to the
129 three problems we mentioned above, and summarized as
130 follows:

- 132 • To avoid noise modeling and estimation, we propose
133 a noval learning based model which directly transform
134 noisy images into clean conuterparts;
- 136 • To learn without paired training images, we perform
137 the learning on paired image patches extracted from
138 unpaired noisy and clean images;
- 139 • To deal with different structures and nise sources, we
140 employ a "divide-and-coquer" strategy on the training
141 data, and for each paired cluster of similar patches, we
142 learn two dictionaries and transformation function for
143 noisy and clean data;
- 145 • The proposed method achieves better performance
146 than other competing methdos on real noisy image de-
147 noising problem.

148 2. Related Work

149 2.1. Couple dictionary learning

150 Coupled dictionary learning (CDL) is a frequently used
151 learning framework for cross-style image synthesis prob-
152 lems, such as image super-resolution, photo-sketch synthe-
153 sis. CDL aims at learning a pair of dictionaries as well as the
154 relationships between the two cross-domain image styles.
155 Hence, the information from the source image style can be
156 applied to synthesize the image at the target style. The
157 relationships are often assumed to be identical mapping (cou-
158 pled) [23], linear mapping (semi-coupled) [24]. Yang et al.
159 [23] assumed that LR image patches have the same sparse
160
161

162 representations as their HR versions do, and proposed a
163 joint dictionary learning model for SR using concatenated
164 HR/LR image features. They later imposed relaxed con-
165 straints on the observed dictionary/coefficient pairs across
166 image domains for improved performance. Wang et al.
167 [24] further proposed a semi-coupled dictionary learning
168 (SCDL) scheme by advancing a linear mapping for cross-
169 domain image sparse representation. Their method has been
170 successfully applied to applications of image SR and cross-
171 style synthesis.

172 2.2. Real Image Denoising

173 To the best of our knowledge, the study of real image
174 denoising can be dated back to the BLS-GSM model [25],
175 in which Portilla et al. proposed to use scale mixture of
176 Gaussian in overcomplete oriented pyramids to estimate the
177 latent clean images. In [13], Portilla proposed to use a cor-
178 related Gaussian model for noise estimation of each wavelet
179 subband. Based on the robust statistics theory [?], the work
180 of Rabie [14] modeled the noisy pixels as outliers, which
181 could be removed via Lorentzian robust estimator. In [15],
182 Liu et al. proposed to use ‘noise level function’ (NLF) to es-
183 timate the noise and then use Gaussian conditional random
184 field to obtain the latent clean image. Recently, Gong et al.
185 proposed an optimization based method [16], which mod-
186 els the data fitting term by weighted sum of ℓ_1 and ℓ_2 norms
187 and the regularization term by sparsity prior in the wavelet
188 transform domain. Later, Lebrun el al. proposed a multi-
189 scale denoising algorithm called ‘Noise Clinic’ [17] for
190 real image denoising task. This method generalizes the NL-
191 Bayes [26] to deal with signal, scale, and frequency depen-
192 dent noise. Recently, Zhu et al. proposed a Bayesian model
193 [18] which approximates the noise via Mixture of Gaussian
194 (MoG) model [20]. The clean image is recovered from the
195 noisy image by the proposed Low Rank MoG filter (LR-
196 MoG). However, noise level estimation is already a chal-
197 lenging problem and denoising methods are quite sensitive
198 to this parameter. Moreover, these methods are based on
199 shrinkage models that are too simple to reflect reality, which
200 results in over-smoothing of important structures such as
201 small-scale text and textures.

202 3. Double Semi-Couple Dictionary Learning

203 In this section, we first formulate the real image denois-
204 ing problem from the perspective of learning based model
205 and then provide the optimization for the problem.

206 3.1. Problem Formulation

207 For real image denoising, we first collect clean natural
208 images and real noisy images for training. Assume the
209 \mathbf{X} and \mathbf{Y} are unpaired clean image patches and real noisy
210 patches. Let the $\mathbf{X} = \mathbf{D}_x \mathbf{A}_x$ and $\mathbf{Y} = \mathbf{D}_y \mathbf{A}_y + \mathbf{V}_y$, where

216 \mathbf{V}_y is the real noise of which we don't know the distribution.
 217
 218

$$\begin{aligned} 219 \quad & \min_{\mathbf{D}_x, \mathbf{D}_y, \mathbf{A}_x, \mathbf{A}_y} E_{data}(\mathbf{X}, \mathbf{D}_x, \mathbf{A}_x) + E_{data}(\mathbf{Y}, \mathbf{D}_y, \mathbf{A}_y, \mathbf{V}_y) \\ 220 \quad & + E_{map}(f_1(\mathbf{A}_x), f_2(\mathbf{A}_y)) + E_{reg}(\mathbf{A}_x, \mathbf{A}_y, f_1, f_2, \mathbf{D}_x, \mathbf{D}_y, \mathbf{V}_y) \end{aligned} \quad (1)$$

221 This framework doesn't need noise modeling and estimation. However, we still model the noise by \mathbf{V}_y for visualization what we have removed during training. The regularization of the noise by $\|\mathbf{V}_y\|_p^p$ can be flexible, that we can penalize it by Frobenius norm, ℓ_1 norm, or any other norms. We employ Frobenius norm here for modeling simplicity. To model the relationship between the representational coefficients, we propose to use two irreversible mapping function f_1 and f_2 . To measure the error, we employ a penalty function F .

$$\begin{aligned} 237 \quad & \min_{\mathbf{D}_x, \mathbf{D}_y, \mathbf{A}_x, \mathbf{A}_y, \mathbf{U}_x, \mathbf{U}_y, \mathbf{V}_y} \|\mathbf{X} - \mathbf{D}_x \mathbf{A}_x\|_F^2 \\ 238 \quad & + \|\mathbf{Y} - \mathbf{D}_y \mathbf{A}_y - \mathbf{V}_y\|_F^2 + \alpha F(f_1(\mathbf{A}_x), f_2(\mathbf{A}_y)) \\ 239 \quad & + \beta_{x1} \|\mathbf{A}_x\|_1 + \beta_{x2} \|\mathbf{A}_x\|_F^2 + \beta_{y1} \|\mathbf{A}_y\|_1 + \beta_{y2} \|\mathbf{A}_y\|_F^2 \\ 240 \quad & \quad (+\gamma_y \|\mathbf{V}_y\|_p^p) \\ 241 \quad & \text{s.t. } \|\mathbf{d}_{x,i}\|_2 = 1, \|\mathbf{d}_{y,i}\|_2 = 1, \forall i. \end{aligned} \quad (2)$$

242 Here, we want to discuss more on the mapping functions f_1, f_2 and the measure function F . The mapping function can be linear or nonlinear transformations. The linear function can be defined as a mapping matrix $f_1(\mathbf{A}_x) = \mathbf{U}_x \mathbf{A}_x$ and $f_2(\mathbf{A}_y) = \mathbf{U}_y \mathbf{A}_y$. The corresponding penalty terms on the mapping matrices are $\|\mathbf{U}_x\|_F^2$ and $\|\mathbf{U}_y\|_F^2$. The nonlinear function can be defined as sigmoid function $f_1(\mathbf{A}_x) = 1/(1 + \exp\{-\mathbf{A}_x\})$. We can also employ "first-linear-then-nonlinear" or "first-nonlinear-then-linear" strategies. Here, we don't have explicit penalty terms for the nonlinear mapping functions. The derivatives of the nonlinear case also need further discussions since it is not easy to obtain closed-form solutions with sigmoid functions. In this paper, we utilize linear transformation matrices as the mapping functions f_1 and f_2 . The measure penalty function is simply defined by Frobenius norm. Hence, the term is defined as $\|\mathbf{U}_x \mathbf{A}_x - \mathbf{U}_y \mathbf{A}_y\|_F^2$. However, this would generate a trivial solution of $\mathbf{U}_x = \mathbf{U}_y = \mathbf{0}$. In order to avoid this case, we propose to use the inverse of the mapping matrices, i.e., \mathbf{U}_x^{-1} and \mathbf{U}_y^{-1} .

243 In summary, we propose a Doubly Inversible and Semi-Coupled Dictionary Learing (DISCDL) model to learn the dictionaries and mapping functions between real noisy im-

ages and latent clean natural images.

$$\begin{aligned} 244 \quad & \min_{\mathbf{D}_x, \mathbf{D}_y, \mathbf{A}_x, \mathbf{A}_y, \mathbf{U}_x, \mathbf{U}_y, \mathbf{V}_y} \|\mathbf{X} - \mathbf{D}_x \mathbf{A}_x\|_F^2 \\ 245 \quad & + \|\mathbf{Y} - \mathbf{D}_y \mathbf{A}_y - \mathbf{V}_y\|_F^2 + \alpha \|\mathbf{U}_x^{-1} \mathbf{A}_x - \mathbf{U}_y^{-1} \mathbf{A}_y\|_F^2 \\ 246 \quad & + \beta_{x1} \|\mathbf{A}_x\|_1 + \beta_{x2} \|\mathbf{A}_x\|_F^2 + \beta_{y1} \|\mathbf{A}_y\|_1 + \beta_{y2} \|\mathbf{A}_y\|_F^2 \\ 247 \quad & \quad (+\gamma_y \|\mathbf{V}_y\|_p^p) \\ 248 \quad & + \lambda_x \|\mathbf{U}_x^{-1}\|_F^2 + \lambda_y \|\mathbf{U}_y^{-1}\|_F^2 \\ 249 \quad & \text{s.t. } \|\mathbf{d}_{x,i}\|_2 = 1, \|\mathbf{d}_{y,i}\|_2 = 1, \forall i. \end{aligned} \quad (3)$$

This model has three major differences when compared with SCDL model.

- We use a matrix \mathbf{V}_y to model the noise, and we don't set any prior distribution on it. This term can help us visualize the noise we learned from the data, i.e., the real noisy images. This make our model fully data-driven. Since our assumption (we have no assumption at all) on noise is more flexible than others', the noise we obtain in our model can be more accurate than other statistical models such as Gaussian or Mixture of Gaussians. Besides, it is time-consuming to fit the noise model from the online data.
- We use two irreversible matrices as the mapping transformations between the coefficients of the real noisy patches and the latent clean patches. This makes our model more flexible than SCDL in which the mapping matrix not explicitly irreversible. Besides, the SCDL can only transform LR images into HG images while our model can transform two different image styles in both direction.
- The constraints on dictionary atoms in our model is strictly $\|\mathbf{d}_{x,i}\|_2 = 1, \|\mathbf{d}_{y,i}\|_2 = 1$ while the CDL model and SCDL model are $\|\mathbf{d}_{x,i}\|_2 \leq 1, \|\mathbf{d}_{y,i}\|_2 \leq 1$. This makes our model more robust on the dictionary learning since both the dictionary atoms and sparse coefficients are interacted with each other. The ≤ 1 constraints would like to make the coefficients larger and dictionary atoms smaller or even vanish. However, in the training stage, we care more about the dictionary atoms and would rather ignore the sparse coefficients.

3.2. Model Optimization

While the objective function in (3) is not convex, it is convex with each variable when other variables are fixed. We employ alternating direction method of multipliers (ADMM) algorithm here. Specifically, we divide the objective function into four sub-problems: 1) updating the sparse coefficients $\mathbf{A}_x, \mathbf{A}_y$; 2) updating the normalized dictionaries $\mathbf{D}_x, \mathbf{D}_y$; 3) updating the noise matrix \mathbf{V}_y ; 4) updating the mapping matirces $\mathbf{U}_x, \mathbf{U}_y$. We discuss the four steps as follows.

324 **3.2.1 Updating \mathbf{A}_x and \mathbf{A}_y**

325
$$\min_{\mathbf{A}_x} \|\mathbf{X} - \mathbf{D}_x \mathbf{A}_x\|_F^2 + \alpha \|\mathbf{U}_x^{-1} \mathbf{A}_x - \mathbf{U}_y^{-1} \mathbf{A}_y\|_F^2 + \beta_{x1} \|\mathbf{A}_x\|_1 + \beta_{x2} \|\mathbf{A}_x\|_F^2, \quad (4)$$

326
$$\min_{\mathbf{A}_y} \|\mathbf{Y} - \mathbf{D}_y \mathbf{A}_y - \mathbf{V}_y\|_F^2 + \alpha \|\mathbf{U}_x^{-1} \mathbf{A}_x - \mathbf{U}_y^{-1} \mathbf{A}_y\|_F^2 + \beta_{y1} \|\mathbf{A}_y\|_1 + \beta_{y2} \|\mathbf{A}_y\|_F^2. \quad (5)$$

334 Take \mathbf{A}_x as an example, the first and second terms above
335 can be combined to form a new optimization problems as
336 follows:

338
$$\min_{\mathbf{A}_x} \|\tilde{\mathbf{X}} - \tilde{\mathbf{D}}_x \mathbf{A}_x\|_F^2 + \beta_{x1} \|\mathbf{A}_x\|_1 + \beta_{x2} \|\mathbf{A}_x\|_F^2, \quad (6)$$

340 where $\tilde{\mathbf{X}} = \begin{pmatrix} \mathbf{X} \\ \sqrt{\alpha} \mathbf{U}_y^{-1} \mathbf{A}_y \end{pmatrix}$ and $\tilde{\mathbf{D}} = \begin{pmatrix} \mathbf{D}_x \\ \sqrt{\alpha} \mathbf{U}_x^{-1} \end{pmatrix}$.
341 For \mathbf{A}_y , it is similar with \mathbf{A}_x .

344
$$\min_{\mathbf{A}_y} \|\tilde{\mathbf{Y}} - \tilde{\mathbf{D}}_y \mathbf{A}_y\|_F^2 + \beta_{y1} \|\mathbf{A}_y\|_1 + \beta_{y2} \|\mathbf{A}_y\|_F^2, \quad (7)$$

347 where $\tilde{\mathbf{Y}} = \begin{pmatrix} \mathbf{Y} - \mathbf{V}_y \\ \sqrt{\alpha} \mathbf{U}_x^{-1} \mathbf{A}_x \end{pmatrix}$ and $\tilde{\mathbf{D}} = \begin{pmatrix} \mathbf{D}_y \\ \sqrt{\alpha} \mathbf{U}_y^{-1} \end{pmatrix}$.
348 These simplified versions have the exactly same formulation
349 as standard sparse coding and can be simply solved by
350 tools such as SPAMS.

352 The \mathbf{U}_x^{-1} and \mathbf{U}_y^{-1} are invertible. This will be discussed
353 in subsection "Updating U".

3.2.2 Updating \mathbf{D}_x and \mathbf{D}_y

357
$$\min_{\mathbf{D}_x} \|\mathbf{X} - \mathbf{D}_x \mathbf{A}_x\|_F^2 \quad \text{s.t.} \quad \|\mathbf{d}_{x,i}\|_2 = 1, \forall i. \quad (8)$$

360
$$\min_{\mathbf{D}_y} \|\mathbf{Y} - \mathbf{D}_y \mathbf{A}_y - \mathbf{V}_y\|_F^2 \quad \text{s.t.} \quad \|\mathbf{d}_{y,i}\|_2 = 1, \forall i. \quad (9)$$

363 These two are quadraically constrained quadratic program
364 (QCQP) problem and can be solved by Lagrange dual tech-
365 niques.

3.2.3 Updating \mathbf{V}_y

369 The noise matrix is initialized as a zero matirx and updated
370 by solving the following probelm:

372
$$\min_{\mathbf{V}_y} \|\mathbf{Y} - \mathbf{D}_y \mathbf{A}_y - \mathbf{V}_y\|_F^2 + \gamma_y \|\mathbf{V}_y\|_F^2 \quad (10)$$

374 This is a ridge regression problem. We can obtain the ana-
375 lytical solution of \mathbf{V}_y by

377
$$\mathbf{V}_y = (\mathbf{Y} - \mathbf{D}_y \mathbf{A}_y) / (1 + \gamma_y). \quad (11)$$

3.2.4 Alternate Updating \mathbf{V}_y

The noise matrix is initialized as a zero matirx and updated
by solving the following probelm:

$$\min_{\mathbf{V}_y} \|\mathbf{Y} - \mathbf{D}_y \mathbf{A}_y - \mathbf{V}_y\|_F^2 \quad (12)$$

This is a standard least square problem. We can obtain the analytical solution of \mathbf{V}_y by

$$\mathbf{V}_y = \mathbf{Y} - \mathbf{D}_y \mathbf{A}_y. \quad (13)$$

3.2.5 Updating \mathbf{U}_x and \mathbf{U}_y

$$\begin{aligned} & \min_{\mathbf{U}_x^{-1}} \alpha \|\mathbf{U}_y^{-1} \mathbf{A}_y - \mathbf{U}_x^{-1} \mathbf{A}_x\|_F^2 + \lambda_x \|\mathbf{U}_x^{-1}\|_F^2 \\ & \min_{\mathbf{U}_y^{-1}} \alpha \|\mathbf{U}_x^{-1} \mathbf{A}_x - \mathbf{U}_y^{-1} \mathbf{A}_y\|_F^2 + \lambda_y \|\mathbf{U}_y^{-1}\|_F^2 \end{aligned} \quad (14)$$

The above problems are also ridge regression problems and have analytical solutions of \mathbf{U}_x and \mathbf{U}_y as follows:

$$\begin{aligned} \mathbf{U}_x^{-1} &= \mathbf{U}_y^{-1} \mathbf{A}_y \mathbf{A}_x^T (\mathbf{A}_x \mathbf{A}_x^T + (\gamma_x/\alpha) \mathbf{I})^{-1} \\ \mathbf{U}_y^{-1} &= \mathbf{U}_x^{-1} \mathbf{A}_x \mathbf{A}_y^T (\mathbf{A}_y \mathbf{A}_y^T + (\gamma_y/\alpha) \mathbf{I})^{-1} \end{aligned} \quad (15)$$

Here, we verify that \mathbf{U}_x^{-1} and \mathbf{U}_y^{-1} are invertible. The \mathbf{U}_x^{-1} and \mathbf{U}_y^{-1} are both initialized as an identity matrix, of suitable dimension, which is inversible. That is, we have $\mathbf{U}_y^{(0)} = \mathbf{I}$ when we compute \mathbf{U}_x^{-1} . If $\mathbf{A}_y \mathbf{A}_x^T$ is inversible, then \mathbf{U}_x^{-1} is inversible. In fact, we have $\mathbf{A}_y, \mathbf{A}_x \in \mathbb{R}^{d \times N}$. d is the dimension of the sample. For a patch of size 8×8 , $d = 64$. The N is the number of samples in the training data. Remember that we have much more samples when compared to the dimension of patches, that is $N \gg d$. It is less likely that $\mathbf{A}_y \mathbf{A}_x^T \in \mathbb{R}^{d \times d}$ has a rank structure lower than d . In other words, $\mathbf{A}_y \mathbf{A}_x^T \in \mathbb{R}^{d \times d}$ is less likely to be singular if we have enough training data. The experiments also confirm our conjecture. Besides, we can also add small disburcation to guarantee that $\mathbf{A}_y \mathbf{A}_x^T \in \mathbb{R}^{d \times d}$ is inversible.

Once \mathbf{U}_x^{-1} is inversible, we can also verify that \mathbf{U}_y^{-1} is inversible in a similar way.

3.3 Real Image Denoising

Two methods:

The first one is that

$$\begin{aligned} & \min_{\mathbf{a}_{x,i}, \mathbf{a}_{y,i}} \|\mathbf{x}_i - \mathbf{D}_x \mathbf{a}_{x,i}\|_2^2 + \|\mathbf{y}_i - \mathbf{D}_y \mathbf{a}_{y,i} - \mathbf{v}_{y,i}\|_2^2 \\ & + \alpha \|\mathbf{U}_x^{-1} \mathbf{a}_{x,i} - \mathbf{U}_y^{-1} \mathbf{a}_{y,i}\|_2^2 \\ & + \beta_x \|\mathbf{a}_{x,i}\|_1 + \beta_{x2} \|\mathbf{a}_{x,i}\|_2^2 + \beta_y \|\mathbf{a}_{y,i}\|_1 + \beta_{y2} \|\mathbf{a}_{y,i}\|_2^2 \\ & + (\gamma_y \|\mathbf{v}_{y,i}\|_1) \end{aligned} \quad (16)$$

and finally we get $\hat{\mathbf{x}}_i = \mathbf{D}_x \hat{\mathbf{a}}_{x,i}$.

432 The second one is to solve
 433

$$\begin{aligned} \min_{\mathbf{a}_{y,i}, \mathbf{v}_{y,i}} & \|\mathbf{y}_i - \mathbf{D}_y \mathbf{a}_{y,i} - \mathbf{v}_{y,i}\|_2^2 + \alpha \|\mathbf{U}_x^{-1} \mathbf{a}_{x,i} - \mathbf{U}_y^{-1} \mathbf{a}_{y,i}\|_2^2 \\ & + \beta_{y1} \|\mathbf{a}_{y,i}\|_1 + \beta_{y2} \|\mathbf{a}_{y,i}\|_2^2 \\ & (+\gamma_y \|\mathbf{v}_{y,i}\|_1) \end{aligned} \quad (17)$$

440 Once we get $\hat{\mathbf{a}}_{y,i}$ from \mathbf{y}_i , $\hat{\mathbf{a}}_{x,i} \approx \mathbf{U}_x \mathbf{U}_y^{-1} \hat{\mathbf{a}}_{y,i}$ and $\hat{\mathbf{x}}_i \approx \mathbf{D}_x \hat{\mathbf{a}}_{x,i}$.
 441

442 Experiments demonstrate that the first method can get
 443 better performance than the second one while the second
 444 one can get faster speed than the first one.
 445

We can also initialized the solution from the second one.

4. The Overall Algorithm

4.1. Pair Sample Construction from Unpaired Samples

451 In cross style transfer methods such as CDL and SCDL,
 452 the authors assume that the two different styles have paired
 453 data, i.e., for each data sample in one style, we can find
 454 paired data sample in the other style. However, in real
 455 world, the data from two different sources may be un-
 456 paired. For example, the real noisy images should not
 457 have groundtruth clean images of the same scene. The real
 458 low-resolution images should not have corresponding high-
 459 resolution images in the real world. The real blurry images
 460 should not have corresponding clear and high quality im-
 461 ages in real world.

462 To deal with unpaired data, we could collect real noisy
 463 images and clean natural images from two different sources.
 464 The real noisy images are from the example images (18 im-
 465 ages) of the Neat Image website while the clean natural im-
 466 ages are from the training set (200 images) of the Berkeley
 467 Segmentation Dataset (BSDS500). To make use of the un-
 468 paired data samples, we employ searching strategy to con-
 469 struct the training dataset. That is, for each noisy image
 470 patch, we utilize the k-Nearest Neighbor (k-NN) algorithm
 471 to find the most similar patch in the clean images as the
 472 paired groundtruth patch. The similarity is measured by the
 473 Euclidean distance (also called squared error or ℓ_2 norm).

4.2. Structural Clustering and Model Selection

474 In fact, different image structures should have differ-
 475 ent influences on dictioanry as well as the mapping func-
 476 tion. Patches with flat region should have low rank struc-
 477 ture within dictionary elements and identity mapping be-
 478 tween noisy and latent clean patches. Patches with com-
 479 plex details should have more comprehensive dictionary el-
 480 ements within dictionary elements and more complex map-
 481 ping function between noisy and clean patches. A single
 482 mapping function cannot deal with all these complex rela-
 483 tionships. Hence, a structural clustering procedure is needed
 484

485 for complex solution. In this paper, we propose to em-
 486 ploy Gaussian Mixture Model to cluster different image
 487 patches into different groups and learn dictionary and map-
 488 ping function for each group.
 489

4.3. Adaptive Iterations of Different Noise Levels

490 For real image denoising, we can perform well on images
 491 which have similar noise levels with the training dataset.
 492 How can we deal with the real noisy images whose noise
 493 levels are higher than the training dataset? The answer is
 494 to remove the noise by more iterations. The input image of
 495 each iteration is the recovered image of previous iteration.
 496 This makes sense since we can still view the recovered im-
 497 age as a real noisy image.
 498

499 This will also bring a second problem, that how we could
 500 automatically terminate the iteration. This can be solved
 501 by two methods. One way is to compare the images be-
 502 tween two iterations and calculate their difference, the it-
 503 eration can be terminated if the difference is smaller than
 504 a threshold. The other way is to estimate the noise level
 505 of the current image and terminate the iterations when the
 506 noise level is lower than a preset threshold. We employ the
 507 second way and set the threshold as 0.0001 in our experi-
 508 ments. In fact, most of our testing images will be denoised
 509 well in one iteration.
 510

4.4. Efficient Model Selection by Gating Network

511 In the Gaussian component selection procedure, if we
 512 employ the full posterior estimation, the speed is not fast.
 513 Our algorithm can be speeded up by introducing the Gating
 514 network model.
 515

5. Experiments

516 We compare with popular software NeatImage which
 517 is one of the best denoising software available. All these
 518 methods need noise estimation which is vary hard to per-
 519 form if there is no uniform regions are available in the test-
 520 ing image. The NeatImage will fail to perform automatical-
 521 ly parameters settings if there is no uniform regions.
 522

5.1. Parameters

523 We don't fine tune the parameters both in the training
 524 and testing datasets.
 525

5.2. Real Image Denoising

526 We compare the proposed method with the famous
 527 BM3D [5] and WNNM [9], Cascade of Shrinkage Fields
 528 (CSF) [10], trainable reaction diffusion (TRD) [12], plain
 529 neural network based method MLP [8], the blind image de-
 530 noising method Noise Clinic [17], and the commercial soft-
 531 ware Neat Image. The RGB images are firstly transformed
 532 into YCbCr channels and restored by these methods. Then
 533

540
541
542
543
544
545
546
547
548
549
550
551
552
553
554
555
556
557
558
559
560
561
562
563
564
565
566
567
568
569
570
571
572
573
574
575
576
577
578
579
580
581
582
583
584
585
586
587
588
589
590
591
592
593
the denoised RGB image is obtained by transforming the restored YCbCr image back.

We evaluate the competing denoising methods from various research directions on two datasets. Both the two datasets comes from the [19]. The first contains 3 cropped images of size 512×512 . The other dataset contains 42 images cropped to size of 500×500 from the 17 images provided in [19]. The 60 images contain most of the scenes in the 17 images [19].

6. Conclusion and Future Work

In the future, we will evaluate the proposed method on other computer vision tasks such as single image super-resolution, photo-sketch synthesis, and cross-domain image recognition. Our proposed method can be improved if we use better training images, fine tune the parameters via cross-validation. We believe that our framework can be useful not just for real image denoising, but for image super-resolution, image cross-style synthesis, and recognition tasks. This will be our line of future work.

References

- [1] Glenn E Healey and Raghava Kondapudy. Radiometric ccd camera calibration and noise estimation. *IEEE Transactions on Pattern Analysis and Machine Intelligence*, 16(3):267–276, 1994. 1, 2
- [2] A. Buades, B. Coll, and J. M. Morel. A non-local algorithm for image denoising. *CVPR*, pages 60–65, 2005. 1
- [3] S. Roth and M. J. Black. Fields of Experts. *International Journal of Computer Vision*, 82(2):205–229, 2009. 1
- [4] M. Elad and M. Aharon. Image denoising via sparse and redundant representations over learned dictionaries. *Image Processing, IEEE Transactions on*, 15(12):3736–3745, 2006. 1
- [5] K. Dabov, A. Foi, V. Katkovnik, and K. Egiazarian. Image denoising by sparse 3-D transform-domain collaborative filtering. *Image Processing, IEEE Transactions on*, 16(8):2080–2095, 2007. 1, 5
- [6] J. Mairal, F. Bach, J. Ponce, G. Sapiro, and A. Zisserman. Non-local sparse models for image restoration. *ICCV*, pages 2272–2279, 2009. 1
- [7] D. Zoran and Y. Weiss. From learning models of natural image patches to whole image restoration. *ICCV*, pages 479–486, 2011. 1
- [8] Harold C Burger, Christian J Schuler, and Stefan Harmeling. Image denoising: Can plain neural networks compete with bm3d? *Computer Vision and Pattern Recognition (CVPR), 2012 IEEE Conference on*, pages 2392–2399, 2012. 1, 5
- [9] S. Gu, L. Zhang, W. Zuo, and X. Feng. Weighted nuclear norm minimization with application to image denoising. *CVPR*, pages 2862–2869, 2014. 1, 5
- [10] U. Schmidt and S. Roth. Shrinkage fields for effective image restoration. *Computer Vision and Pattern Recognition (CVPR), 2014 IEEE Conference on*, pages 2774–2781, June 2014. 1, 5
- [11] J. Xu, L. Zhang, W. Zuo, D. Zhang, and X. Feng. Patch group based nonlocal self-similarity prior learning for image denoising. *2015 IEEE International Conference on Computer Vision (ICCV)*, pages 244–252, 2015. 1
- [12] Yunjin Chen, Wei Yu, and Thomas Pock. On learning optimized reaction diffusion processes for effective image restoration. *Proceedings of the IEEE Conference on Computer Vision and Pattern Recognition*, pages 5261–5269, 2015. 1, 5
- [13] J. Portilla. Full blind denoising through noise covariance estimation using gaussian scale mixtures in the wavelet domain. *Image Processing, 2004. ICIP '04. 2004 International Conference on*, 2:1217–1220, 2004. 1, 2
- [14] Tamer Rabie. Robust estimation approach for blind denoising. *Image Processing, IEEE Transactions on*, 14(11):1755–1765, 2005. 1, 2
- [15] C. Liu, R. Szeliski, S. Bing Kang, C. L. Zitnick, and W. T. Freeman. Automatic estimation and removal of noise from a single image. *IEEE Transactions on Pattern Analysis and Machine Intelligence*, 30(2):299–314, 2008. 1, 2
- [16] Zheng Gong, Zuowei Shen, and Kim-Chuan Toh. Image restoration with mixed or unknown noises. *Multiscale Modeling & Simulation*, 12(2):458–487, 2014. 1, 2
- [17] M. Lebrun, M. Colom, and J.-M. Morel. Multiscale image blind denoising. *Image Processing, IEEE Transactions on*, 24(10):3149–3161, 2015. 1, 2, 5
- [18] Fengyuan Zhu, Guangyong Chen, and Pheng-Ann Heng. From noise modeling to blind image denoising. *The IEEE Conference on Computer Vision and Pattern Recognition (CVPR)*, June 2016. 1, 2
- [19] Seonghyeon Nam, Youngbae Hwang, Yasuyuki Matsushita, and Seon Joo Kim. A holistic approach to cross-channel image noise modeling and its application to image denoising. *Proc. Computer Vision and Pattern Recognition (CVPR)*, pages 1683–1691, 2016. 1, 2, 6, 7, 8
- [20] C. M. Bishop. *Pattern recognition and machine learning*. New York: Springer, 2006. 1, 2
- [21] S. J. Kim, H. T. Lin, Z. Lu, S. Ssstrunk, S. Lin, and M. S. Brown. A new in-camera imaging model for color computer vision and its application. *IEEE Transactions on Pattern Analysis and Machine Intelligence*, 34(12):2289–2302, Dec 2012. 2
- [22] Yanghai Tsin, Visvanathan Ramesh, and Takeo Kanade. Statistical calibration of ccd imaging process. *Computer Vision, 2001. ICCV 2001. Proceedings. Eighth IEEE International Conference on*, 1:480–487, 2001. 2
- [23] Jianchao Yang, John Wright, Thomas S Huang, and Yi Ma. Image super-resolution via sparse representation. *IEEE transactions on image processing*, 19(11):2861–2873, 2010. 2

648 Table 1. Average PSNR(dB) results of different methods on 3 real noisy images captured by Canon EOS 5D mark3 at ISO3200 in [19]. 702

649 650 651 652 653 654 655 656 657 658 659 660 661 662 663 664 665 666 667 668 669 670 671 672 673 674 675 676 677 678 679 680 681 682 683 684 685 686 687 688 689 690 691 692 693 694 695 696 697 698 699 700 701	Image	Noisy	BM3D	WNNM	CSF	TRD	MLP	Noise Clinic	Neat Image	Ours
	1	37.00	37.08	37.09	37.46	37.51	32.91	38.76	37.68	38.63
	2	33.88	33.95	33.95	34.90	35.04	31.94	35.69	34.87	35.96
	3	33.83	33.85	33.85	34.15	34.07	30.89	35.54	34.77	35.51
	Average	34.90	34.96	34.96	35.50	35.54	31.91	36.67	35.77	36.70

656 Table 2. Average SSIM results of different methods on 3 real noisy images captured by Canon EOS 5D mark3 at ISO3200 in [19]. 710

657 658 659 660 661 662 663 664 665 666 667 668 669 670 671 672 673 674 675 676 677 678 679 680 681 682 683 684 685 686 687 688 689 690 691 692 693 694 695 696 697 698 699 700 701	Image	Noisy	BM3D	WNNM	CSF	TRD	MLP	Noise Clinic	Neat Image	Ours
	1	0.9345	0.9368	0.9372	0.9599	0.9607	0.9043	0.9689	0.9600	0.9712
	2	0.8919	0.8848	0.8951	0.9159	0.9187	0.8498	0.9427	0.9308	0.9434
	3	0.9128	0.9136	0.9136	0.9254	0.9279	0.8635	0.9476	0.9463	0.9529
	Average	0.9131	0.9117	0.9153	0.9337	0.9358	0.8725	0.9531	0.9457	0.9558

- [24] Shenlong Wang, Lei Zhang, Yan Liang, and Quan Pan. Semi-coupled dictionary learning with applications to image super-resolution and photo-sketch synthesis. *Computer Vision and Pattern Recognition (CVPR), 2012 IEEE Conference on*, pages 2216–2223, 2012. 2
- [25] J. Portilla, V. Strela, M.J. Wainwright, and E.P. Simoncelli. Image denoising using scale mixtures of Gaussians in the wavelet domain. *Image Processing, IEEE Transactions on*, 12(11):1338–1351, 2003. 2
- [26] M. Lebrun, A. Buades, and J. M. Morel. A nonlocal bayesian image denoising algorithm. *SIAM Journal on Imaging Sciences*, 6(3):1665–1688, 2013. 2

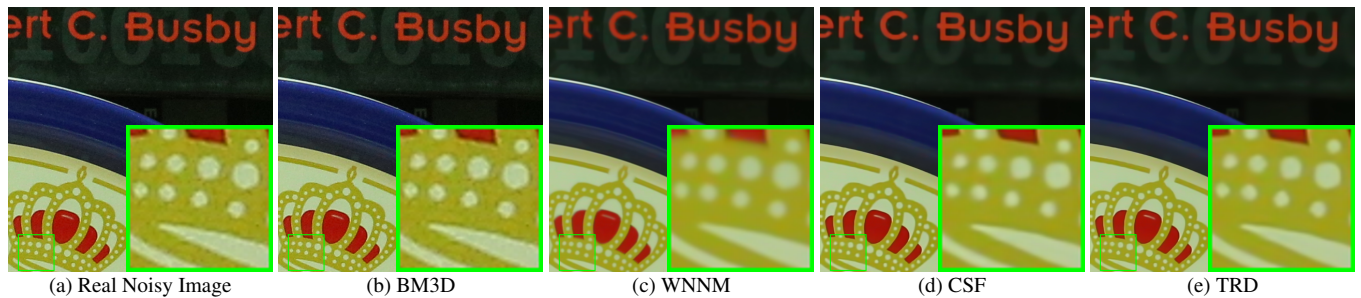
756
757
758
759
760
761
762
763
764
765
766810
811
812
813
814
815
816
817
818
819
820
821
822
823
824
825
826
827
828
829
830
831
832
833
834
835
836
837
838
839
840
841
842
843
844
845
846
847
848
849
850
851
852
853
854
855
856
857
858
859
860
861
862
863

Figure 1. Denoised images of the old image "5dmark3iso32001" by different methods. The images are better to be zoomed in on screen.

777

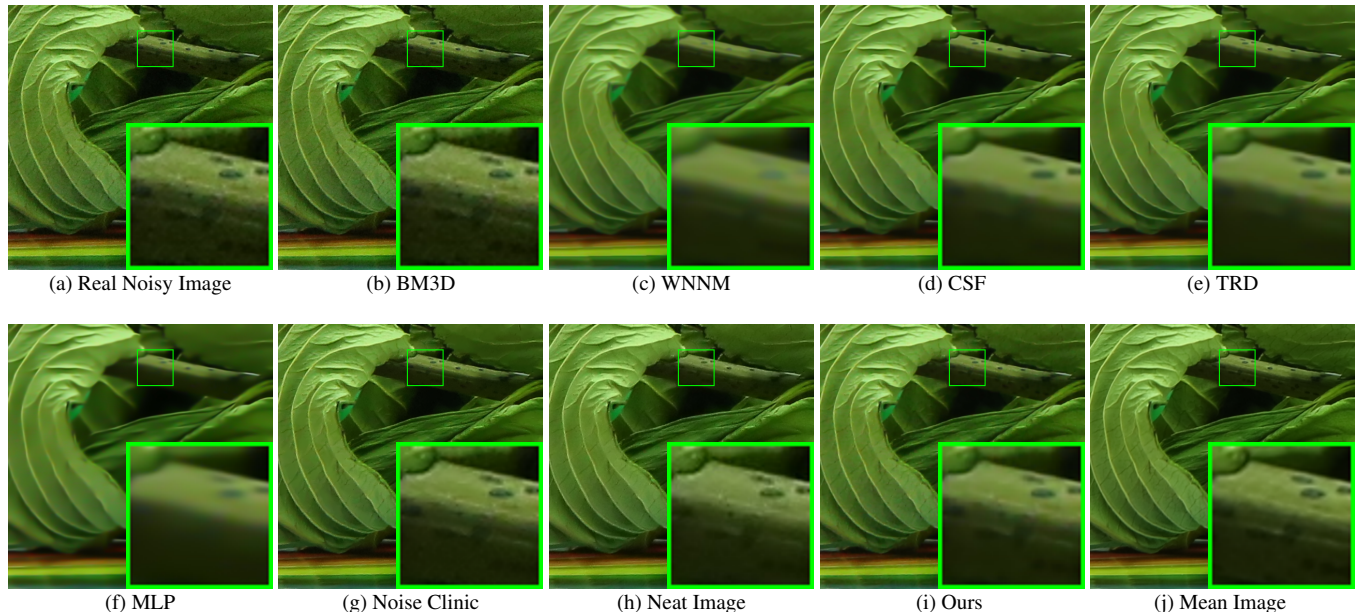


Figure 2. Denoised images of the old image "5dmark3iso32002" by different methods. The images are better to be zoomed in on screen.

801

802

803

Table 3. Average PSNR(dB) and SSIM results of different methods on 42 cropped images from 17 real noisy images in [19].

Measure	Noisy	BM3D	WNNM	CSF	TRD	MLP	Noise Clinic	Neat Image	Ours
PSNR	34.36	34.36	34.40	36.11	36.05	34.41	37.68	36.58	36.15
SSIM	0.8552	0.8553	0.8577	0.9215	0.9211	0.9012	0.9470	0.9145	0.9236

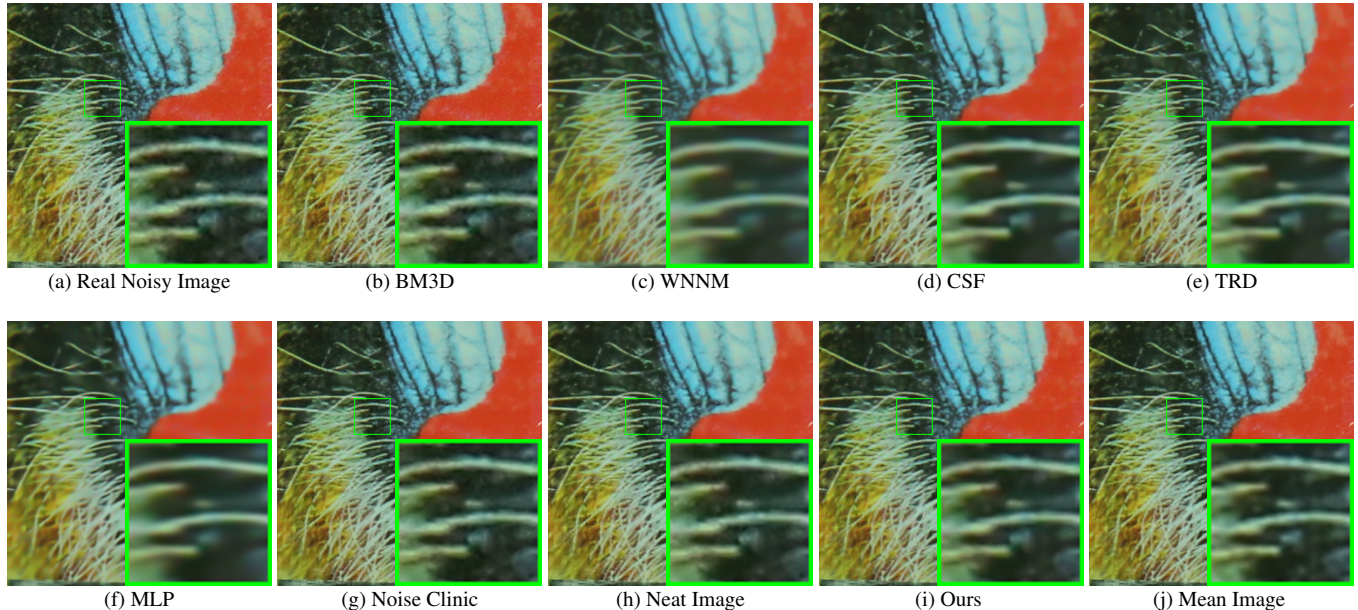
864
865
866
867
868
869
870
871
872
873
874
875
876
877
878
879
880918
919
920
921
922
923
924
925
926
927
928
929
930
931
932
933
934

Figure 3. Denoised images of the old image "5dmark3iso3200_3" by different methods. The images are better to be zoomed in on screen.

901
902
903
904
905
906
907
908
909
910
911
912
913
914
915
916
917954
955
956
957
958
959
960
961
962
963
964
965
966
967
968
969
970
971